Origin of Corona-Dominated Topographic Rises on Venus

SUZANNE E. SMREKAR AND ELLEN R. STOFAN
Jet Propulsion Laboratory, California Institute of Technology, MS 183-501,
4800 Oak Grove Dr., Pasadena, CA 91209
e-mail: ssmrekar@cythera.jpl.nasa.gov

Both large-scale mantle upwellings, comparable to terrestrial hotspots on Earth, and smaller scale mantle upwellings, known as coronae, occur on Venus. Corona-dominated rises have many of the characteristics of large scale mantle upwellings, or hotspots, such as broad topographic rises greater than 1000 km in diameter and large positive gravity anomalies. Due to the presence of clusters of 3 to 8 coronae, three large volcanic rises (or hotspots) on Venus have been classified as corona-dominated rises (CDRs): Themis, Eastern Eistla and Central Eistla Regiones. CDRs have been interpreted to result from the break-up of a large scale plume. Comparison of the topographic morphology for individual coronae at Themis and Eastern Eistla Region to a model of corona evolution indicate they are in varying stages of evolution. At Eastern Eistla Regio all the coronae have essentially the same topographic morphology, consistent with a late stage of evolution and the presence of a depleted mantle layer at depth. The complex deformation sequences and stratigraphic relationships both between coronae and with respect to the regional plains observed at all three rises indicate a prolonged origin. This observation, as well as the varying stages of evolution, rule out the previously proposed interpretation of corona-dominated rises as a manifestation of the break-up of a large scale mantle upwelling, which requires essentially simultaneous formation of the coronae. Instead we suggest that other large topographic rises are the manifestation of deep mantle plumes, likely to originate at the core-mantle boundary, and that CDRs are clusters of coronae that originate at a shallower interface, perhaps at an upper-lower mantle boundary. Using top and bottom-loading flexural models to fit the gravity/topography admittance spectrum for each of the three CDRs yield elastic thickness estimates that are 10-15 km greater for bottom-loading at longer wavelengths than top-loading at shorter wavelengths. Estimates of elastic thickness assuming top-loading are 10, 12, and 22 km and 20, 25, and 35 km from bottom-loading for Eastern Eistla, Central Eistla, and Themis Regiones, respectively. We believe the bottom-loading elastic thickness estimates are more reliable because using a top-loading model when both types of loading are present yields an unrealistically low elastic thickness estimate. As there is no obvious source of surface loading at

either Themis or at Eastern Eistla, we interpret the top-loading admittance signature to be a result of delamination of the lower lithosphere depressing the surface, which is consistent with the observed coronae morphologies.

Key words: Venus, corona, gravity, delamination, hotspots

INTRODUCTION

The relatively large resurfacing age of ~750 My and the very small percentage of craters that are modified by volcanism and tectonism (McKinnon *et al.* 1997) imply that the present day level of geologic activity on Venus is low. A central question in the study of Venus is how does a planet with a similar bulk density and thus radioactive heat production as Earth lose its heat without ongoing resurfacing of large regions. Studies of coronae, small scale mantle upwellings, and larger scale volcanic rises (or hotspots) are a critical part of deciphering the present day state of Venus both because the loading environments offer an opportunity to constrain elastic thickness and because coronae may play a significant role in heat loss on Venus through associated delamination of the lower thermal lithosphere (Smrekar and Stofan 1997).

Coronae are unique to Venus and are defined by their approximately circular annulus of fractures. There are 362 coronae, ranging in size from approximately 100 to 1000 km in diameter (Stofan *et al.* 1992). There are a comparable number of 'stealth' coronae that lack a fracture annulus, making them difficult to observe using radar data, but which are identified by having the same range of topographic signatures as coronae with fractures (Tapper *et al.* 1998). The large number of coronae make them an important tool for trying to understand the thickness of the lithosphere globally and its evolution over time (Johnson and Solomon 1996).

Here we examine the relationship between coronae and large volcanic rises, the surface manifestation of large-scale mantle upwellings. Large volcanic rises on Venus have been classified into three groups: rift-dominated rises, corona-dominated rises, and volcano-dominated rises (Stofan *et al.* 1995). Stofan *et al.* (1995) interpreted the predominance of coronae at corona-dominated volcanic rises to possibly reflect small-scale convection in the lithosphere induced by

the rising plume or instabilities and break up of the plume head (e.g. Griffiths and Campbell 1991), creating small-scale diapiric upwellings that form coronae.

The three corona-dominated rises (CDRs), Themis, Eastern Eistla and Central Eistla Regiones, are clusters of coronae that lie on broad topographic rises greater than 1000 km in diameter and have positive gravity anomalies characteristic of hotspots. In comparison to other volcanic rises, they tend to have lower topographic swell heights, lower peak gravity anomalies, and typically fewer shield volcanoes. Each of the corona-dominated rises differ in the number of associated coronae and in the morphologies of those coronae.

In this paper geologic mapping studies detail the stratigraphy within each of the three areas as well as the relationship to the surrounding plains. The topographic morphologies of the individual coronae are compared to a recent study of corona formation to estimate the evolutionary stage of individual coronae (Smrekar and Stofan 1997). We examine the gravity and topography signature and the geologic history of each of the three corona-dominated rises in detail. Admittances studies using the latest 180 degree and order spherical harmonic gravity and topography fields (Konopliv *et al.* 1998; Rappaport *et al.* 1998) are used to determine elastic thicknesses in the three regions. Where the resolution is adequate, geoid-to-topography ratios for the larger coronae are used to compare the apparent depths of compensation between coronae. Admittance spectra at CDRs can be interpreted as indicating a relatively thin elastic lithosphere or as a dynamic signature due to delamination. Below we argue that the signature is best interpreted as evidence for delamination of the lower lithosphere beneath coronae. Finally, we discuss the implications of this study for the relationship of CDRs to other large volcanic rises and reexamine the plume head break-up hypothesis.

GEOLOGY OF CORONA-DOMINATED RISES

Themis Regio

Themis Regio is a broad regional high with a diameter of about 2000 km and a height of about 0.5 km (note this height estimate is revised from that given in Stofan *et al.* (1995)). At Themis

Regio, eight major coronae have been mapped (Fig. 1a, Table 1). The eight coronae range in diameter from 275 to 675 km. Themis Regio is unique in that it lies at the terminus of the Parga Chasma corona chain (Stofan *et al.* 1992; Stofan *et al.* 1995) and is the only CDR that contains significant extensional deformation. Fractures and graben are much less common than along the rest of Parga Chasma, and are embayed by corona-related flows. Although later stage corona volcanism postdates extension, rift and corona formation have overlapped in time.

The topography of the coronae have been classified following the scheme presented in Smrekar and Stofan (1997) (see discussion below). Four are plateaus, two have rims surrounding an interior high, one has a rim surrounding an interior raised above the surrounding terrain, and another is a depression partially surrounded by a rim (Table 1). Two coronae have outer rises surrounding deep troughs, and are sites proposed to be subduction trenches (Schubert and Sandwell 1995). Most of the coronae in Themis Regio have extensive associated flow deposits. Flows range in morphology from sheet-like to digitate, and both embay and are cut by corona-related deformation.

Mapping of Themis Regio has permitted the delineation of some stratigraphic relationships. Early-stage flows from Tacoma, Ukemochi and a corona centered at 37°S, 293°E (TH5) overlie regional plains to the north of Themis Regio, indicating that formation of these coronae generally postdated formation of these plains. Plains units originating from unknown sources within Themis Regio are both overlain by corona deposits and overlie the regional plains, suggesting that rise formation in general has postdated regional plains formation. Corona flows also overlie plains units to the south, west and east of Themis Regio.

Individual coronae in Themis Regio have a range in complexity of morphology and in the amount of associated volcanism. In comparison to the other two CDRs, coronae at Themis Regio tend to have more associated flows and small edifices. Coronae such as Ukemochi, Shiwanokia and TH5 underwent multiple stages of volcanism and deformation. At Ukemochi, an earlier episode of interior deformation was followed by annulus formation, which in turn was followed by another episode of interior deformation. Initial more sheet-like flows have been followed by

more digitate flows, and the formation of a small edifice on the annulus. This edifice has been subsequently deformed by continuing annular deformation. The complex, long-duration histories of these coronae are consistent with corona histories described by Copp *et al.* (1998).

Some stratigraphic relationships between coronae at Themis Regio can also be determined. Flows from Shiwanokia, the largest corona, overlie the southern flows from the corona centered at 38.5°S, 284°E (TH2). Flows from TH2 overlie deposits from TH3 (centered at 34.5°S, 284°E), from Rigatona, and Tacoma corona, while Rigatona flows also overlie TH3 deposits. Flows from TH5 overlie deposits from Tacoma, Tamiyo and Ukemochi coronae. However, some flows from Ukemochi overlie Tamiyo flows, while other Tamiyo flows overlie Ukemochi deposits. The great complexity of the coronae in this region and their abundant volcanic deposits suggest long histories. In general, stratigraphic relationships between episodes of volcanism can sometimes be observed, but the relative ages of volcanic flows cannot be used to determine if the apparently older corona ceased all activity prior to emplacement of the youngest flows. In fact, the apparently older corona may have begun its formation after the apparently younger feature.

Eastern Eistla Regio

Eastern Eistla Regio is a volcanic rise approximately 1700 km in diameter and approximately 1 km in height. There are five coronae in eastern Eistla Regio, the largest of which is Pavlova Corona (Fig. 2a, Table 2). Eastern Eistla Regio is not associated with a major rift system, though it is partially surrounded by small-scale fracture belts. One of the unique aspects of Eastern Eistla is that the four coronae on the rise are very similar in size, morphology, and volcanic and tectonic characteristics. All of them have interior radial fractures which are atypical of most coronae. These type of features have been interpreted as dike swarms overlying an intrusion (Head *et al.* 1992).

Tectonic deformation indicates that Calakomana (IAU Provisional name), the fifth corona that lies just off the rise to the south, is the oldest corona in the region. Most, but not all, corona deposits have been deformed by wrinkle ridges. Two coronae to the northeast of Calakomana, an

unnamed corona (hereafter referred to as Corona EE3) and Isong Corona (IAU Provisional), have radial fractures on their rims, although their rims are less continuous than the rims of the western coronae. Radially fractured terrain in the interior of Corona EE3 is embayed by flows. The wrinkle ridges in the northern plains terminate and are deflected away from the NW rim of Corona D, implying that wrinkle ridge formation occurred after corona rim formation. The northern flows of Isong Corona overlay the southern flows of Corona EE3, indicating that at least some geologic activity at Isong postdates volcanism at Corona EE3.

The two western coronae, an unnamed corona hereafter referred to as Corona EE1 and Pavlova corona (IAU Provisional), have radial fractures on nearly continuous rims, which are embayed by relatively smooth interior flows. Both coronae also have late-stage radial rift-like fractures located near their centers. Some of these fractures cut into the annular rims. Both of the coronae also have exterior volcanism that generally originates at small edifices on the corona rims. Corona EE1 is the only one of the two that displays any concentric fracturing, with a few fractures on its eastern rim. The western coronae appear to have rims composed of a different unit than that of the surroundings, indicating that the rims were fractured and uplifted prior to the surrounding volcanism. The timing of interior volcanism, however, is not easily constrained.

Some stratigraphic relationships can be determined for the coronae in Eastern Eistla Regio. Both Calakomana and Corona EE3 formed prior to wrinkle ridge formation in this region, indicating that they began forming prior to the other three coronae. Corona EE1 western flows appear to postdate western flows from Pavlova, but their mottled appearance and large volume make stratigraphic correlations difficult. The Corona EE1 eastern flows are mostly postdated by northern flows of Pavlova, but some small lobes appear to overlay Pavlova flows. This suggests that Pavlova has some of the most recent flows in the area, but it is also apparent that volcanism at Corona EE1 and Pavlova Corona may have been concurrent, and that both coronae have had a protracted history.

The northern flows of Pavlova provide the only cross-regional correlation in Eastern Eistla. The wrinkle ridges which terminate against the rim of Corona EE3 are partially overlain by the

Pavlova flows, which implies Pavlova northern flows postdate Corona EE3 rim formation. Unfortunately, this relationship is of minimal significance because Isong Corona flows cannot be correlated with Pavlova or Corona EE1 flows, as all are younger than Corona EE3 rim formation. Gravity data (Johnson *et al.* 1997) suggests that the western coronae are younger, but geologic mapping only indicates that corona rim formation preceded volcanism at the other three coronae. No firm stratigraphic relationship between Pavlova and the two eastern coronae can be established from our mapping. A strong possibility is that the coronae are of a similar age and the western corona are simply more volcanically active.

Central Eistla Regio

Central Eistla Regio is approximately 1200 km in diameter and 1 km in height. It has two large coronae, with diameters of 300 and 345 km, a volcanic shield, and a smaller corona with a diameter of 170 km (Fig. 3a, Table 3). The region has been previously described by McGill (1994; 1998). McGill did not classify Sappho as a corona as it has abundant radiating volcanic flows. However, it does have a well-defined annulus of fractures, and many coronae have well-developed flow aprons (Roberts and Head 1993; Stofan *et al.* 1997). While large shields also have abundant radiating flows, they have distinctive summit characteristics and shapes that differ from coronae. Sappho has a raised rim and an interior depression that lies above the surrounding terrain. Therefore, we consider Sappho to be a corona. Although Anala Mons was originally classified as a corona-like feature (Stofan *et al.* 1992), it has a shield-shape and a radial summit structure similar to other volcanic edifices on Venus. The other large corona, Nehalennia, has a partial rim with very chaotic interior topography; the small corona, Sunrta, is a depression.

Sappho and Nehalennia Coronae both have associated volcanism, with Sappho having a greater amount. McGill (1994) mapped four units associated with Sappho, all interpreted to be volcanic in origin. Sunrta Corona has no apparent volcanic deposits with the possible exception of some small flows in the interior. Deposits from Nehalennia and Sappho overlie surrounding plains; fractures from Sunrta cut plains units. Flows from Anala Mons, a large shield volcano in Central

Eistla Regio, also overlie plains deposits. This indicates that late-stage volcano and coronae flows generally postdated local plains deposits, but it is impossible to determine whether they began forming before or after plains formation based on the radar images. Flows from Anala Mons also overlie flows extending to the south of Sappho and are diverted by Sappho topography (McGill 1994), but it is not possible to determine which feature began forming first.

Central Eistla Regio differs from the other CDRs in that it has fewer coronae and has a large shield volcano, making it transitional to volcano-dominated rises such as Bell Regio. It has two zones of extensional deformation, though neither are as well-developed as Parga Chasma. The abundant volcanism at both Anala Mons and at Sappho result in its volcanic style differing from the other CDRs, which tend to be dominated by more sheet-like or distributed corona deposits.

MORPHOLOGY OF CORONA TOPOGRAPHY

While each of the three areas studied is a corona-dominated rise, the coronae at each rise vary greatly in morphology (Fig. 2). Central Eistla Regio and Themis Regio have multiple types of coronae (i.e., plateaus, depressions); Eastern Eistla Regio has basically one type of corona. Smrekar and Stofan (1997) developed a model of corona formation that includes delamination of the lower lithosphere as a result of mantle upwelling and that can produce the full range of observed corona topographic groups. A low density layer of depleted mantle beneath the thermal lithosphere is also included in some cases. The presence of such a layer is consistent with all of the observed topographic forms and is required to produce one class, rim only coronae. The wide range of corona topographic shapes have been interpreted to indicate varying stage of evolution rather than effects of variations in plume or lithospheric properties (Smrekar and Stofan 1997). In this model, corona rims can be produced by resistance to delamination at depth (where a central high or low is also present) or by isostatic rebound of a depleted mantle layer following thermal equilibration of the cold delaminating lower lithosphere. The morphology of the coronae in Eastern Eistla Regio is thus most consistent with the late to very late stages of

corona evolution, produced by upwelling and delamination, possibly in the presence of a depleted mantle layer.

The morphologies of the coronae at the other CDRs are representative of the full range of stages of corona evolution. Most are consistent with the presence of a depleted mantle layer and delamination, but do not require it (Smrekar and Stofan 1997). The two coronae in Themis Regio with deep troughs and outer rises either require delamination or subduction and are thus in a mid to late stage of formation. On the basis of morphology, the youngest coronae in Themis Regio may be Shiwanokia, TH2, Ukemochi, and Tamiyo. These coronae are all plateaus or approximately plateaus. Plateaus can form either in an intermediate stage of evolution, just as the plume begins to cool and topography relaxes, or during late stage evolution as inward migration of the delaminating lower lithosphere causes crustal thickening (Smrekar and Stofan 1997). The multiple deformation and volcanic events observed at many of these coronae suggest that a late stage of evolution may be more likely.

GRAVITY AND TOPOGRAPHY SIGNATURES

A large gravity high is associated with the broad topographic highs at each of the CDRs (Fig. 3). Data are 1° by 1° grids derived from the Mgnp180u field, which significantly better resolution than prior spherical harmonic fields (Konopliv *et al.* 1998). The latest topographic field is also a significant modification from past fields, with changes most apparent at intermediate wavelengths of several thousand kilometers (Rappaport *et al.* 1998). Each region has a comparable gravity anomaly range of approximately -20 to 80 mgals. Many of the coronae with significant topography correspond to smaller gravity highs (Fig. 3).

Gravity/Topography Admittance

Forward modeling of the gravity and topography data is performed in the spectral domain rather than in the spatial domain to allow for greater discrimination between compensation mechanisms and the estimation of elastic thickness. The spectral admittance approach (Dorman and Lewis 1970) assumes that the relationship between gravity and topography is both linear and

isotropic. Uncorrelated parts of the signals are treated as noise. The admittance function is defined as cross spectrum of the gravity with topography over the power spectrum of the topography

$$Z(k) = (\mathrm{Re} \langle G(k) H(k)^* \rangle) / (\langle H(k) H(k)^* \rangle)$$

where k is the wavenumber, equal to 2π/wavelength, the angular brackets denote averaging over discrete wavenumber bands, $G(k)$ is the Fourier transform of the gravity, $H(k)$ is the Fourier transform of the topography, *Re* indicates the real part of the Fourier transform, and * indicates the complex conjugate (e.g. McNutt 1979). The gravity and topography data are mirrored prior to taking the Fourier transform to minimize edge effects (McNutt 1983). The uncertainty in each estimate of ∂Z_n is given by

$$dZ = (\langle G-ZH \rangle \langle G^*-ZH^* \rangle)^{1/2} / (\langle H H^* \rangle)^{1/2}$$

Each data point shown in Fig. 3 is the average of information over a given wavenumber band; error bars indicate the uncertainty in each band.

The gravity/topography admittance spectra for the three regions are shown in Fig. 4. At Eastern Eistla Regio, the areas are split into two halves to examine differences between the eastern and western coronae, which have been interpreted as different in age (Johnson *et al.* 1996). The two sets of model curves shown in each plot include the effects of flexure of the elastic lithosphere; solid lines show bottom loading at depth (and thus at long wavelengths) to represent a plume at depth and dashed lines show top-loading curves to account for the effect of loading near the surface by volcanoes or other loads. Both models include deflection of a crustal layer, which has a density contrast of 400 kg/m^3 relative to the mantle. This model was first developed for terrestrial hotspots by McNutt and Shure (1986) and then applied to large volcanic rises (Smrekar 1994; Smrekar *et al.* 1997). Isostatic compensation curves (not shown) have a relatively constant slope and do not provide a good fit to the data for any of the three regions.

The bottom-loading model provides an excellent fit to the spectrum for Themis Regio at wavelengths between 700 and 1500 km (Fig. 4a), giving an elastic thickness value of 30±5 km. The bottom-loading model does not fit the data very well for Central Eistla and Eastern Eistla

Regiones (Fig. 4b,c,d), but is still better than the isostatic compensation model. The estimated values of elastic thickness from a bottom load are 20±5 km at Eastern Eistla and 25±5 km at Central Eistla. Although the data provides a relatively poor fit to the model in these regions, fits to larger regions centered in these areas, which thus include more long wavelength information, are consistent with these values. The long wavelength values of apparent depths of compensation (ADCs) are 95-105 km for the three regions, assuming a crustal thickness of 30 km. As discussed below, crustal thicknesses have been varied to obtain a good fit in Fig. 4, but in Table 4 a value of 30 km is used to determine the ADC for comparison to values obtained for other regions. The ADC has been interpreted to indicated the depth to a thermal anomaly at the base of the lithosphere (e.g. Simons *et al.* 1994; Moore and Schubert 1995). However, more complex convective models, some with temperature-dependent viscosity, have shown that the ADC does not provide a reliable estimate of the thickness of the thermal lithosphere (e.g. Moresi and Parsons 1995; Solomatov and Moresi 1996). Thus here we calculate apparent depths of compensation simply as a general means to compare the long-wavelength portion of the spectra between regions.

The admittance spectrum for each of the three areas has a steep slope at wavelengths less than 600-1000 km. At Themis, the best fit is for a crustal thickness of 10 km and an elastic thickness of 22 km (Fig. 4a). At Central Eistla, the best fit is for a crustal thickness of 20 km and an elastic thickness of 12 km (Fig. 4d). At Eastern Eistla Regio, we have divided the region into a western and eastern half to determine if there are any differences between the two primary clusters of coronae. For the western half, which includes Pavlova Corona, a good fit is obtained for a crustal thickness of 20 km and an elastic thickness of 10 km. For the eastern side, including Isong Corona, the same values give a good fit. These values have an uncertainty of at least ±5 km as elastic thickness and crustal thickness can be traded off, with smaller values of elastic thickness giving larger crustal thicknesses (see below). An additional uncertainty is that the exact shape of the curve is affected by the exact size and location of the chosen wavenumber bins. Within the uncertainties in the fits, there is no difference between the parameters estimated for the two sides

of Eastern Eistla Regio. Analyzing a larger area at both Central and Eastern Eistla Regiones, thereby including more long-wavelength information, results in a better fit of the data to a bottom-loading model. The spectrum for all of Eastern Eistla is shown in Fig. 5. The resulting elastic thicknesses estimates agree with those for smaller regions (Fig. 4). When the large box (Fig. 2) is used for Eastern Eistla, the same apparent depth of compensation, 75 km, is obtained as that found by Schubert *et al.* 1994).

The differences in the admittance curves for the three regions and the sensitivity of the top-loading model to crustal and elastic thickness variations are illustrated in Fig. 5. The admittance spectra for each of the three areas have similar short wavelength slopes, but considerably different offsets in wavelength. Both crustal thickness and elastic thickness affect the slope and offset of the top loading model, but over the relevant range of parameters, slope is primarily controlled by crustal thickness and offset is primarily controlled by elastic thickness. The uncertainty due to the trade-off between these two parameters is no more than ±5 km. For example, the model curve for a crustal thickness of 10 km and an elastic thickness of 12 km provides the best fit to the short wavelength spectrum for Central Eistla Regio. However, the curve for a crustal thickness of 10 km and an elastic thickness of 15 km nearly falls within the error bars. Similarly, small variations in crustal thickness would produce curves that fall within the error bars. The estimated value of crustal thickness from the top-loading model is used in the bottom-loading model from which the ADC is derived (Fig. 4). To calculate the ADC assuming a typical crustal thickness value of 30 km (Grimm and Hess 1997) the difference between the smaller crustal thickness and 30 km can simply be added to the ADC. For example, the ADC at Themis using a crustal thickness of 10 km is 80 km; for a crustal thickness of 30 km the ADC is 100 km.

Comparisons to Other Volcanic Rises and Coronae. Admittance curves with steep slopes at short wavelengths are also observed for other large volcanic rises, including Bell, Atla, and Beta Regiones (Smrekar 1994; Phillips *et al.* 1997; Simons *et al.* 1997), as well to some extent in the highland plateau regions of Ovda and Phoebe Regiones (Simons *et al.* 1997). A summary of

elastic thicknesses, crustal thicknesses, and ADC values from this and other studies for all of the large topographic rises is given in Table 4. Note that values given from Simons *et al.* (1997) tend to cover a larger range because they analyzed a large number of areas and did not attempt to optimize the fit for each one. The elastic thickness estimates from the short-wavelength top-loading model fit to the admittance spectra for CDRs are comparable to the low end of those for the large topographic rises. The elastic thickness estimates from the long-wavelength, bottom-loading model are instead on the high end of the 10-40 km range for large volcanic rises, as well as the typical 10-35 km range of coronae (Johnson and Sandwell 1994; Johnson *et al.* 1997). The apparent depths of compensation are also on the low side relative to other rises. However, these values cannot be directly translated into lithospheric thickness since they are very sensitive to viscosity structure, as discussed above.

Interpretation. In each case, the elastic thickness obtained from the long-wavelength bottom-loading model is larger than that obtained from the short-wavelength top load, although the bottom-loading fit to the data at Central and Eastern Eistla Regiones is not as good as at Themis Regio. There are several ways to interpret this result. The first is that there is local thinning of the elastic lithosphere in the vicinity of the top load, as suggested for Bell Regio (Smrekar 1994) and for a terrestrial hotspot, the Bermuda Rise (Sheehan and McNutt 1989). Alternatively, the small values of elastic thickness may be due to fitting a top-loading only model to a region in which there is a large proportion of bottom-loading relative to top-loading (Forsyth 1985). The difference in the estimates of elastic thickness from the two models is 10-15 km and could easily be due to the presence of bottom-load with a mass approximately twice that of the top-load. Lastly, the accuracy of the elastic thickness estimate, as with any estimate for a possible hotspot region, may be affected by dynamic topography due to a mantle plume (Smrekar *et al.* 1997), as will be discussed below.

First we consider the possibility that the elastic thickness locally thinned in the vicinity of a top-load, such as a volcano. There are two problems with this interpretation. The first is that small values of elastic thickness due to thinning by a vigorous mantle plume are expected to be

accompanied by high topography, a large associated gravity anomaly, and extensive volcanism due to additional pressure release melting (Smrekar and Parmentier 1996; Nimmo and McKenzie 1997). This is not the case for the Corona-Dominated Rises. Instead, the gravity anomalies and topographic rises found at the CDRs are smaller than at any of the other large volcanic rises, with the single exception of Dione Regio (Stofan *et al.* 1995). We have not specifically estimated the volume of the shield volcano Anala Mons in Central Eistla. However, the total volume is likely to be significantly less that at other volcanic rises. Thus we suggest that the bottom-loading estimates of elastic thickness are likely to be more accurate for CDRs than the top-loading values because there is no associated evidence of a thin lithosphere.

The second problem with the interpretation that small elastic thickness estimates are due to local thinning in the vicinity of a top-load is the absence of an obvious top-load at Eastern Eistla. In all models of corona formation, the topography of corona is created by uplift of the lithosphere. The uplifted lithosphere does not constitute a load. On Venus, where erosion rates are very low, the primary source of surface loads are volcanic edifices. Although low relief flows are present at Eastern Eistla and Themis, it is unlikely that a distributed load with variable thickness would be detectable in the admittance signature since it would have a variable strength and be spread over a range of wavelengths. Further, those wavelengths are likely to be much smaller than the wavelength of ~400 km where the resolution falls off.

We next discuss the possible sources of bottom-loading and dynamic signatures. An obvious source of bottom-loading is mantle plumes, on the scale of the coronae and possibly on the scale of the topographic rises (see discussion below). The possible short-wavelength admittance signature due to dynamic effects of a long-wavelength plume is illustrated in Smrekar *et al.* (1997). In that example, the dynamic signature can be fit using a bottom-loading only flexure model.

Models of coronae formation that include delamination of the lower lithosphere predict a gravity/topography admittance spectrum comparable to those found for the three CDRs. The gravity signature of a corona with a delaminating lower lithosphere is the similar to a top-loading

model because the topography is pulled downward just as top load depresses the surface. The temperature and velocity fields shown in Fig. 6 are for a corona upwelling model with a mantle Rayleigh number of 10^5, and a viscosity contrast of 10^4 distributed between the mantle viscosity of 4.5×10^{18} Pa s at the interior temperature, 1300°C and 10^{21} Pa s at a temperature of 1100°C within the thermal lithosphere. The resulting corona has a diameter of approximately 600 km, comparable to the larger coronae in Themis and Eastern Eistla. Further details of this finite element modeling approach to modeling mantle upwellings in general are given in Smrekar and Parmentier (1996) and to coronae specifically in Smrekar and Stofan (1997). The predicted topography and admittance are shown for three output times at 7.7, 12.6, and 13.6 m.y. after the start of the calculation in Fig. 7 and 8. At 7.7 m.y., the plume has begun to interact with the lower lithosphere (Fig. 6a) and has produced minor uplift of the surface (Fig. 7). The admittance spectra at this time has a shallow slope (Fig. 8), comparable to other models of upwellings that are best fit with a bottom-loading model (Smrekar et al. 1997).

Delamination of the lower lithosphere causes the shape of the admittance curve to change. At 12.6 m.y., the delaminating lower lithosphere has descended approximately 50 km into the mantle (Fig. 6b), depressing the surface topography (Fig. 7) and steepening the admittance curve (Fig. 8). A good fit to the predicted admittance is obtained by an elastic thickness of 10 km and a crustal thickness of 50 km (Fig. 8). One million years later, the delaminating ring has sunk approximately 100 km further into the mantle (Fig. 6c). The resulting topography is only slightly more depressed (Fig. 7), but the admittance slope is considerably steeper (Fig. 8) and is well fit by a crustal thickness of 15 km and an elastic thickness of 30 km. In the 1000-1500 km range, the spectra also generally follow the bottom-loading curve for an elastic thickness of 30 km, a crustal thickness of 30 km, and an ADC of approximately 100 km, comparable to observed spectra for CDRs.

Clearly the dynamic behavior of the delamination process results in predicted values of elastic thickness and crustal thickness that can change significantly as the delamination progresses, making it difficult to constrain the exact elastic thickness. As with the fits to actual data, there is

a trade off in elastic thickness and crustal thickness that introduces an error of approximately ±5 km in both elastic thickness and crustal thickness. Although there is no crustal layer, elastic layer or imposed lid, the behavior of the high viscosity lid is similar to that of an elastic layer. The range of 10-30 km for the elastic thickness are generally consistent with the 100 km thick, high viscosity thermal lithosphere. The near surface thermal gradient of approximately 12°/km gives a temperature of 750°C at a depth of 20 km. Although the base of the elastic lithosphere is not solely controlled by temperature, elastic behavior ceases roughly in the range of 500-750°C (McNutt 1984).

The interpretation that the small values of elastic thickness are due to local thinning in the vicinity of a top-load is problematic because of the absence of concentrated loads such as volcanoes at Eastern Eistla and at Themis. One might also expect greater topographic uplift and increased volumes of volcanism relative to areas with thicker elastic thicknesses. This is not observed. We prefer the interpretation that the steep short wavelength portion of the admittance spectrum is a result of the delamination of the lower lithosphere. Theoretically, pulling down on the lithosphere produces a signature that is identical to that of pushing down on the lithosphere. The delamination interpretation is further corroborated by the morphology of the coronae at each of the CDRs, which in many cases has only been predicted by models that include delamination (Smrekar and Stofan 1997). Within this interpretation, elastic thicknesses obtained from bottom loading at long wavelengths are thus more reliable than those from the short wavelength portion of the spectra.

Finally we note that the other region of Venus where this difference between estimates of elastic thickness from the top-loading and bottom-loading models is observed is Bell Regio. Although classified as a volcano-dominated rise because of the prominent shield volcano Tepev Mons (Stofan *et al.* 1995), Bell Regio is transitional to the CDRs. To the east of Tepev Mons, there is a prominent feature which has been classified as both a volcano and as a corona. Another corona lies to the north. The rise topography contains two overlapping highs, much like Eastern Eistla Regio.

DISCUSSION

There is a general lack of correlation between stratigraphic age and topographic morphology that indicates corona formation is an extremely complex process. The complex sequence of deformation and volcanism observed at most coronae imply a long duration for formation (Copp *et al.* 1998). There is also considerable evidence that coronae at a given large volcanic rise do not form synchronously. Wrinkle ridges in the regional plains at Eastern Eistla Regio are stratigraphically younger than two corona and older than three others. At Themis and Central Eistla Regiones there are coronae in apparently varying stages of evolution. Stratigraphic relationships among coronae at Themis Regio are also very complex.

Previous studies have suggested that corona-dominated rises are a result of instabilities formed simultaneously due to break-up of a single large plume head as it impinges on the lithosphere (Griffiths and Campbell 1991; McGill 1994; Stofan *et al.* 1995). The broad topographic rise and associated gravity anomaly at each of these regions suggests the presence of an underlying plume. However, the variety of evolutionary stages of corona formation observed at Themis and Central Eistla Regiones, as well as the complex geologic history at all three regions, supports the hypothesis that small-scale upwellings are distributed in time rather than nearly simultaneous. The primary differences between CDRs and other large topographic rises are the lower volcanic volumes and lower topographic swells (Stofan *et al.* 1995). With the exception of Anala Mons in Central Eistla, CDRs lack shield volcanoes. Note that models of corona formation produce coronae by uplift of the surface not by volcanic construction (e.g. Stofan *et al.* 1991; Janes *et al.* 1992; Janes and Squyres 1995; Koch and Magna 1996; Cyr and Melosh 1996; Smrekar and Stofan 1997).

CDRs may be analogous in some sense to the more minor 'hotspots' observed on Earth, where there is clearly a source of hot material at depth but there is not an obvious case for a mantle plume arising from the core mantle boundary (Wessel 1997). McNutt *et al.* (1997) found in that in the Austral islands, previously considered to be a single hotspot track, there are three distinct volcanic sources lacking a consistent age progression. They interpret this data to indicate

the presence of a diffuse upwelling with volcanoes located at tectonically weak zones. A primary difference between CDRs and terrestrial regions of diffuse upwelling is the presence of coronae, whose locations do not appear to be structurally controlled. Although coronae are not found on Earth it is possible that such small scale upwellings do occur on Earth but simply do not produce the same type of surface deformation due to the presence of a low viscosity zone (Smrekar and Stofan 1997) which acts to diffuse the upwelling and reduce surface deformation. It has been suggested that coronae are Rayleigh-Taylor type instabilities (Tackely and Stevenson 1991; Hamilton and Stofan 1996) but it is not clear where such instabilities would form. The base of the lithosphere is too shallow an interface. A boundary between upper mantle and lower mantle convection is a more likely interface, based simply on the size range of coronae. Instabilities at the upper-lower mantle boundary might be induced by heating from a lower mantle plume that could not penetrate the interface. The more diffuse swells on Earth may also originate from a similar shallow source.

The difference between CDRs and other large topographic rises may be related to their source region. Other large topographic rises may be due to large plumes arising at the core-mantle boundary; CDRs appear to result from a cluster of smaller scale upwellings that arise from a shallower depth. This hypothesis may also account for greater abundance of shield volcanoes at non-CDRs. Large volumes of pressure-release melting are required to produce the large shield volcanoes common at other large topographic rises (Stofan *et al.* 1995). From studies of terrestrial hotspots and volcanism, there are several factors that are known to control pressure release melting at hotspots. Thinner lithosphere and higher plume temperature both contribute to higher melt volumes (e.g. Smrekar and Parmentier 1996; Nimmo and McKenzie 1997). Chemistry of the melt region is another factor (Cordery *et al.* 1997). Here we suggest that vigorous mantle plumes, perhaps from the core-mantle boundary, that form the non-CDR rises have higher temperatures and buoyancy fluxes and thus produce the very large volumes of pressure release-melting needed to produce large shield volcanoes. The smaller plumes that produce coronae are less likely to produce such massive volumes of pressure-release melting.

In contrast, McGovern and Solomon (1998) argue that coronae form on thin lithosphere and volcanoes form on thick lithosphere based on their modeling of volcano formation which requires relatively thick lithosphere to produce volcanoes. They also suggest that elastic thickness estimates for coronae are typically smaller than for volcanoes. However there is considerable overlap in the elastic thickness estimates for coronae and large volcanic rises. McGill (1994) interpreted the geologic history of Central Eistla Regio to be consistent with a swarm of plumes, first forming coronae and then volcanoes as the lithosphere thickened over time. His timing of volcano formation versus corona formation was partially dependent on his interpretation of Sappho as a volcano. The thickening of the lithosphere was interpreted to result from cooling following global catastrophic resurfacing. In revisiting the morphology of Sappho and Anala Mons, McGill (1998) interpreted them to be coronae which formed on top of volcanoes as the lithosphere thinned. However, late-stage annulus formation at Sappho is typical of other coronae (e.g. Copp *et al.* 1998) and the overall shape of Sappho does not require it to be a volcano. On other large volcanic rises, coronae and volcanoes can be found with variable stratigraphic ages. At Western Eistla Regio, Idem-kuva Corona postdated the formation of Gula Mons (Copp *et al.* 1998). Stofan *et al.* (1997) interpreted the similarity of coronae at different geologic settings, which might be expected to have different lithospheric thicknesses, to indicate that factors other than lithospheric thickness must influence the formation of coronae vs. large volcanoes.

The estimates of elastic thickness for CDRs obtained here fall within the range found for large volcanic rises, coronae, and Venus overall (Phillips *et al.* 1997; Simons *et al.* 1997). Phillips *et al.* (1997) used the range of elastic thickness estimates and reasonable assumptions for the lithospheric rheology to estimate the thickness of the thermal lithosphere. They find that the average thermal lithosphere thickness is likely to be Earth-like (~100-150 km) or slightly thicker. Studies of the bounds placed on thermal lithospheric thickness by the formation of pressure-release melting to form shield volcanoes at large volcanic rises yield a similar range (Smrekar and Parmentier 1996; Nimmo and McKenzie 1997). A major question for Venus is how does the planet lose its heat given an Earth-like lithospheric thickness and no global system of plate

tectonics. The evidence for delamination at many of the coronae at these CDRs is consistent with coronae contributing a significant fraction of Venus' heat flow, with delamination accounting for part of the 'missing' heat budget on Venus (Smrekar and Stofan 1997).

CONCLUSIONS

The complex deformation sequences, stratigraphic relationships, and varying evolutionary stages of individual coronae indicate that long duration, small scale upwellings impinged asynchronously on the bottom of the lithosphere to form the coronae at CDRs. Comparisons of coronae topographic morphology to a model of corona formation (Smrekar and Stofan 1997) indicate that coronae are in range of stages of evolution at Themis and Central Eistla Regiones, while at Eastern Eistla, all the coronae are in a very late stage of evolution. On this basis we eliminate the break-up of a single large-scale mantle plume as an explanation for CDRs. We suggest that the primary difference between CDRs and other large volcanic rises may be to due to different sources for the mantle upwellings, with plumes at other rises originating from the core-mantle boundary and a series of smaller plumes from shallower depths, perhaps the upper-lower mantle boundary, forming CDRs. Further, the lesser terrestrial hotspots, where the volcanic centers have been shown to have a non-sequential time of formation with respect to plate motion (McNutt *et al.* 1997; Wessel 1997), may form in the same manner as CDRs. Such regions on Earth would not be likely to form coronae at the surface because the low viscosity zone under the oceanic lithosphere is likely to diffuse small scale upwellings. Delamination is also likely to be suppressed by asthenospheric flow on Earth.

Analysis of the gravity and topography data indicate that the loading processes, like the geologic histories, are complex in these regions. However, the admittance spectrum is similar in each region. For each area , the elastic thickness estimate found by fitting a bottom-loading model at long-wavelength is larger by 10-15 km than the results of a top-loading model fit to the short-wavelength part of the spectrum. We interpret this difference to indicate that both top and bottom-loading are present at short wavelengths, but that the top-loading only model results in

an underestimate of the elastic thickness (Forsyth 1985). For this reason, the bottom-loading values of elastic thickness, 10, 12, and 22 km, at Eastern Eistla, Central Eistla, and Themis Regiones, respectively, are likely to be more reliable. The elastic thicknesses estimates found at CDRs are consistent with Earth-like values rather than the 'thick' lithosphere required by some models of resurfacing of Venus (e.g. Turcotte 1993).

Despite the top-loading signature in the data for all three regions, only Central Eistla has an obvious source of top-loading in the form of Anala Mons. Delamination of the lower lithosphere, which is inferred from the coronae morphology, is believed to be the source of the top-loading signature found in each region. However, models of corona formation with delamination that predict the observed top-loading signature show that dynamic effects can result in unreliable elastic thickness estimates if static top-loading models are applied. The observed top-loading signature in addition to the corona morphology further support the hypothesis that coronae contributing to heat loss on Venus through both upwellings and delamination (Smrekar and Stofan 1997).

TABLE I
Coronae in Themis Regio Coronae.

Coronae	Center (Lat°S, Lon°E)	Diameter (km)	Topographic Morphology	Topo. Class
Shiwanokia	42.0, 279.0	675	Partial rim, irregular plateau	2/3a
TH2	38.5, 284.0	275	Irregular plateau	2
TH3	34.5, 284.0	325x225	Depression, partial rim	8
Tacoma	37.0, 288.0	500	Partial rim, inner high	3b
TH5	37.0, 293.0	375	Partial outer rise, trough, irregular plateau	5
Ukemochi	39.0, 296.0	325	Partial outer rise, trough, plateau	5
Tamiyo	36.0, 298.5	375x330	Irregular plateau, partial rim	2
Rigatona	33.5, 279.0	300	Double rim	3b/7

TABLE II
Coronae in Eastern Eistla Regio.

Coronae	Center (Lat°N, Lon°E)	Diameter (km)	Topographic Morphology	Topo. Class
EE1	18.5, 37.5	320	Rim surrounding interior high (depression)	3b
Isong	12.0, 49.5	540	Rim surrounding interior high (depression)	3b
EE3	17.0, 48.0	750 x350	Rim Only	7
Pavlova	14.5, 39.5	500	Rim Only	7
Calakomana	6.5,43.5	575	Rim Only	7

TABLE III
Coronae in Central Eistla Regio.

Coronae	Center (Lat°N, Lon°E)	Diameter (km)	Topographic Morphology	Topo. Class
Nehalennia	14.0, 10.0	345	Rim, irregular interior	7
Sappho	14.2, 15.4	300	Rim, raised interior	3a
Sunrta	8.3, 11.7	170	Partial rim, depression	4
Anala Mons	11.0,14.0	240	Shield volcano	NA

TABLE IV
Elastic and crustal thicknesses and ADCs for large volcanic rises.

Volcanic Rise	Elastic Thickness (km)	Crustal Thickness (km)	ADC (km)
Atla Regio	25[3]-30[1,2,4]	16[2], 30[1,3], 40[4]	175[5]
Beta Regio	10-20[4], 27.5[2]	20-40[4]	225[5]
Bell Regio	15-30[1,4], 40*	20-40	125[5]
W. Eistla	25[6]	30[6]	200[5]
Dione Regio	-	-	130[5]
Imdr Regio	-	-	260[5]
E. Eistla Regio	10, 20*	29	95
C. Eistla Regio	12, 25*	20	105
Themis Regio	22, 35*, 10-20[4]	10, 20-40[4]	100

Values with no superscript are from this study; an * indicates a second estimate of elastic thickness found from the long wavelength portion of the admittance. Values for Eastern Eistla Regio are an average of those found for the eastern and western halves. Low resolution in the gravity do not permit estimates of elastic or crustal thickness for Imdr and Dione Regiones. Elastic and crustal thicknesses estimates from is study have an uncertainty of approximately ±5 km. Uncertainties for apparent depths of compensation are approximately ±15 km. References: 1) Smrekar 1994; 2) McKenzie and Nimmo 1997; 3) Phillips *et al.* 1997; 4) Simons *et al.* 1997; 5) Stofan *et al.* 1995; 6) Smrekar *et al.* 1997.

ACKNOWLEDGMENTS

We thank Todd Fleming, Daniel Nunes, and An Nguyen for their contributions to this work through the NASA Planetary Geology and Geophysics Undergraduate Research Program. We also thank Walter Kiefer and an anonymous reviewer for comments that significantly improved the paper.

REFERENCES

Copp, D.L., J.E. Guest and E. R. Stofan 1998. New insights into corona evolution: Mapping on Venus. ***J. Geophys. Res.*** **103,** 19,401-19,418.

CORDERY, M. J., G. F. DAVIES, AND I. H. CAMPBELL 1997. Genesis of flood basalts from eclogite-bearing mantle plume. *J. Geophys. Res.* **102**, 20, 179-20, 197.

CYR, K. E., AND H. J. MELOSH 1996. Tectonic patterns and regional stresses near venusian coronae. *Icarus* **102**, 175-184.

DORMAN, L. M., AND B. T. R. LEWIS 1970. Experimental isostasy, I: Theory of the determination of the earth's isostastic response to a concentrated load, *J. Geophys. Res.* **75**, 3357-3365.

FORSYTH, D. Subsurface loading and Estimates of the Flexural Rigidity of Continental Lithosphere, *J. Geophys. Res.* **90**, 12,623-12,632.

GRIFFITHS, R. W., AND I. H. CAMPBELL 1991. Interaction of mantle plume heads with the Earth's surface and onset of small-scale convection, *J. Geophys. Res.* **96**, 18, 295-18, 310.

GRIMM, R. E., AND P. C. HESS 1997. The crust of Venus, in *Venus II*, eds. S. W. BOUGHER, D. M. HUNTEN AND R. J. PHILLIPS, University of Arizona Press, Tucson, pp. 1205-1244.

HAMILTON, V. E., AND E. R. STOFAN 1996. The geomorphology and evolution of Hecate Chasma, Venus, *Icarus* **121**, 171-194.

HEAD, J. W., L. S. CRUMPLER, J. C. AUBELE, J. E. GUEST, AND R. S. SAUNDERS 1992. Venus volcanism: Classifications of volcanic features and structures, associations, and global distribution from Magellan data, *J. Geophys. Res.* **97**, 13, 153-13,198.

JANES, D. M., SQUYRES, S. W., BINDSCHADLER, D. L., BAER, G., SCHUBERT, G., SHARPTON, V. L., AND STOFAN, E. R. 1992. Geophysical models for the formation and evolution of coronae on Venus. *J. Geophys. Res.* **92**, 16,055-16,068.

JANES, D. M. AND SQUYRES, S. W. 1995. Viscoelastic relaxation of topographic highs on Venus to produce coronae, *J. Geophys. Res.* **100**, 21, 173-21, 187.

JOHNSON, C. L., AND D. T. SANDWELL 1994. Lithospheric flexure on Venus, *Geophys. J. Int.* **119**, 627.

JOHNSON, C. L., AND S. C. SOLOMON 1996. Variations in lithospheric properties on Venus from Coronae and Chasmata, *Lunar Planet. Sci. Conf.* **XXVII**, 607-608.

JOHNSON, C. L., P. J.. MCGOVERN, S. C. SOLOMON, D. T. SANDWELL, AND M. SIMONS 1997. Lithospheric thickness variations on Venus, *Venus Chapman Conf.*, abs. **15**.

KONOPLIV, A. S., W. B. BANERDT, AND W. L. SJOGREN 1998. Venus Gravity: 180th degree and Order Model, this issue.

KOCH, D. M. AND M. MAGNA 1996. Neutrally buoyant diapirs-A model for Venus Corona, *Geophys. Res. Lett.* **23**, 225-228.

McGill, G. E. 1994. Hotspot evolution and Venusian tectonic style, *J. Geophys. Res.* **99**, 23, 194-23, 162.

MCGILL, G. E. 1998. Central Eistla Regio: Origin and relative age of topographic rises. *J. Geophys. Res.* **103**, 5889-5896.

MCGOVERN, P. J., AND S. C. SOLOMON 1998. Growth of large volcanoes on Venus from line to sight accelerations, *Icarus* **103**, 11, 071-11, 101.

MCKENZIE, D., AND F. NIMMO 1997. Elastic thickness estimates for Venus from line to sight accelerations, *Icarus*, **130**, 198-216.

MCKINNON, W. B., K. J. ZAHNLE, B. A. IVANOV, H. J. MELOSH 1997. Cratering on Venus: Models and observations, in *Venus II*, eds. S. W. BOUGHER, D. M. HUNTEN, and R. J. PHILLIPS, University of Arizona Press, Tucson, pp. 969-1014.

McNUTT, M. 1979. Compensation of oceanic topography: An application of the response function technique to the Surveyor area. *J. Geophys. Res.* **84**, 7589-7598.

MCNUTT, M. K. 1983. Influence of plate subduction on isostatic compensation in northern California. *Tectonics* **2**, 399-415.

MCNUTT, M. K. 1984. Lithospheric flexure and thermal anomalies. J. Geophys. Res. **89**, 11,180-11,194.

MCNUTT, M., AND L. SHURE 1986. Estimating the compensation depth of Hawaiian swell with linear filters. *J. Geophys. Res.* **91**, 13,915-13,923.

MCNUTT, M. K., D. W. CARESS, J. REYNOLDS, K. A. JORDAHL, AND R. A. DUNCAN 1997. Failure of plume theory to explain midplate volcanism in the southern Austral islands, *Nature* **389**, 470-482.

MOORE, W. B., AND G. SCHUBERT 1995. Lithospheric thickness and mantle/lithosphere density contrast beneath Beta Regio, Venus. *Geophys. Res. Lett.* **22**, 429-432.

MORESI, L., AND B. Parsons 1995. Interpreting gravity, geoid, and topography for convection with temperature dependent viscosity: application to surface features on Venus. *J. Geophys. Res.* **100**, 21,155-21,171.

NIMMO, F. AND D. MCKENZIE 1997. Modeling plume-related melting, uplift and gravity on Venus. *Earth Planet. Sci. Lett.* **145**, 109-123.

PHILLIPS, R. J., S. W. BOUGHER, D. M. HUNTEN, C. L. JOHNSON, S. L. MACKWELL, P. MORGAN, D. T. SANDWELL, M. T. ZUBER 1997. Lithospheric mechanics and dynamics of Venus, in *Venus II*, eds. University of Arizona Press, Tucson pp. 931-965.

RAPPAPORT, N. J., A. S. KONOPLIV, A. B. KUCINSKAS, P. G. FORD 1998. An improved 360 degree and order model of Venus topography, this issue.

ROBERTS, K. M., AND J. W. HEAD 1993. Large-scale volcanism associated with coronae on Venus: Implications for formation and evolution. *Geophys. Res. Lett.* **20**, 1111-1114.

SCHUBERT, G., W. B. MOORE, AND D. T. SANDWELL 1994. Gravity over coronae and chasmata on Venus. *Icarus* **117**, 173-196.

SCHUBERT, G., AND D. T. SANDWELL 1995. A global survey of possible subduction sites on Venus. *Icarus* **117**, 173-196.

SHEEHAN, A. F., AND M. K. MCNUTT 1989. Constraints on thermal and mechanical structure of the oceanic lithosphere at the Bermuda Rise from geoid height and depth anomalies. *Earth Planet. Sci. Lett.* **93**, 377-391.

SIMONS, M., B. H. HAGER, AND S. C. SOLOMON 1994. Global variations in the geoid:topography admittance of Venus. *Science* **264**, 798-803.

SIMONS, M., S. C. SOLOMON, AND B. H. HAGER 1997. Localization of gravity and topography: Constraints on the tectonics and mantle of dynamics of Venus. *Geophys. J. Int.* **13**, 24.

SMREKAR, S. E. 1994. Evidence for active hotspots on Venus from analysis of Magellan gravity data. *Icarus* **112**, 2-26.

SMREKAR, S. E., AND PARMENTIER, E. M. 1996. The interaction of mantle plumes with surface thermal and chemical boundary layers: Application to hotspots on Venus. J. Geophys. Res. **101**, 5397-5410.

SMREKAR, S. E., W. S. KIEFER, AND E. R. STOFAN 1997. Large volcanic rises on Venus in *Venus II*, eds. S. W. BOUGHER, D. M. HUNTEN, AND R. J. PHILLIPS, University of Arizona Press, Tucson. pp. 845-878.

SMREKAR, S. E., AND E. R. STOFAN 1997. Coupled upwelling and delamination: A new mechanism for coronae formation and heat loss on Venus, *Science* **277**, 1289-1294.

SOLOMATOV, V. S., AND L. MORESI 1996. Stagnant lid convection on Venus. *J. Geophys. Res.* **101**, 4737-4753.

STOFAN, E. R., D. L. BINDSCHADLER, J. W. HEAD, AND E. M. PARMENTIER 1991. Corona structures on Venus: Models of origin. *J. Geophys. Res.* **96**, 20,933-20,946.

STOFAN, E. R., V. L. SHARPTON, G. SCHUBERT, G. BAER, D. L. BINDSCHADLER, D. M, JANES, AND S. W. SQUYRES 1992. Global distribution and characteristics of coronae and related features on Venus: Implications for origin and relation to mantle processes. *J. Geophys. Res.* **97**, 13,347-13,378.

STOFAN, E. R., S. E. SMREKAR, D. L. BINDSCHADLER AND D. A. SENSKE 1995. Large topographic rises on Venus: Implications for mantle upwelling. *J. Geophys. Res.* **100**, 23,317-23,327.

STOFAN, E. R., D. L. BINDSCHADLER, V. E. HAMILTON, D. M. JANES, AND S. E. SMREKAR 1997. Coronae on Venus: Morphology and origin in *Venus II*, eds. S. W. BOUGHER, D. M. HUNTEN AND R. J. PHILLIPS, University of Arizona Press, Tucson, pp. 931-965.

TACKLEY, P. J., AND D. J. STEVENSON 1991. The production of small Venusian coronae by Rayleigh-Taylor instabilities in the uppermost mantle. Eos: Tans. *AGU* **72**, 287.

TAPPER, S. W., E. R. STOFAN, AND J. E. GUEST 1998. Preliminary analysis of an expanded corona database. *Lunar Planet. Sci. XXIX*, Abstract #1104.

TURCOTTE, D. L. 1993. An episodic hypothesis for Venusian tectonics. *J. Geophys. Res.* **98**, 17,061-17,068.

WESSEL, P. 1997. Sizes and ages of seamounts using remote-sensing - Implications for intraplate volcanism. *Science* **277**, 802-805.

FIGURE CAPTIONS

Figure 1. Magellan radar images for Themis (a), Eastern Eistla (b), and Central Eistla (c) Regiones. Themis Regio (a) is a volcanic rise with a diameter of about 2000 km. The eight major coronae are Shiwanokia (Sh), Corona TH2 (2), Corona TH3 (3), Rigatona (R), Tacoma (T), Corona TH5 (5), Ukemochi (Uk), and Tamiyo (Ta) (see Table 1). (b) Eastern Eistla Regio is a approximately 1800 km in diameter. There are four major coronae in Eastern Eistla Regio, the largest of which is Pavlova Corona (P) (approximately 500 km across). The other coronae on the rise are Corona EE1 (1), Isong (2), and Corona EE3 (3). The northern half of Calakomana Corona (5), located to the south of the rise, can be seen in the image above. (c) The rise at Central Eistla Regio is about 1200 km in diameter. Sappho Corona (S) is approximately 300 km across. Two other coronae in Central Eistla Regio are Nehalennia (N) and Sunrta (Su). Anala Mons (A\), a shield volcano, is about 240 km across.

Figure 2. Topographic profiles derived from the ARCDR data for coronae in Themis (TH2, Shiwanokia, and TH5), Eastern Eistla (Isong and Pavlova), and Central Eistla (Sappho and Suntra). These profiles represent the range of coronae topography found in the CDRs.

Figure 3. Gravity and topography data from spherical harmonic fields for Themis, Eastern Eistla, and Central Eistla Regiones. The locations of the topographic profiles in Fig. 2 are shown. Note that the topography data in this figure is from a lower resolution sampling than that used to create Fig. 2. Coronae locations are also shown in as the first letter of their names or as numbers correlated to the text and tables 1-3.

Figure 4. Gravity/topography admittances for Themis (a), Eastern Eistla (western side) (b), Eastern Eistla (eastern side) (c), and Central Eistla (d). Solid lines are bottom loading models. Dash-dot lines are top loading models. The vertical dotted line is the approximate cut-off of the

resolution in gravity data, as determined by the cross over in the strength of the spherical harmonic field relative to the data errors (Konopliv *et al.* 1998). Detailed analysis of the error in individual orbits of gravity data indicate that this is a lower bound on the true resolution in the data. In practice the cut-off in resolution is usually apparent in the drop off of the admittance spectra.

Figure 5. The effects of varying crustal thickness and elastic thickness on model admittance curves. Slope is most sensitive to crustal thickness and horizontal offset is most sensitive to elastic thickness. Compare for example the curve for a crustal thickness of 10 km and an elastic thickness of 15 km with that for a crustal thickness of 10 km and an elastic thickness of 12 km. Admittance spectra for the three CDRs are also shown for comparison.

Figure 6. The temperature and velocity fields for a finite element model of corona formation. Temperature is indicated by color, from 500°C at the top surface to 1350°C in the plume. White contours occur at temperatures of 1000, 1100, 1200, 1280, 1300, 1320, and 1350°C. Arrows show the flow direction, with length proportional to the magnitude. At 7.7 m.y., the plume is beginning to thin the lithosphere slightly (Fig. 6a). At 12.6 m.y., delamination of the lower lithosphere has begun (Fig. 6b), and by 13.6 m.y. has reached a depth of approximately 150 km beneath the base of the lithosphere.

Figure 7. The predicted topography fof the corona model time steps of 7.7 m.y. (dotted line), 12.6 m.y. (dash-dot line), and 13.6 m.y. (solid line), corresponding to those illustrated in Fig. 6.

Figure 8. The admittance spectra calculated from the predicted gravity and topography for the three model time steps seen in Figures 6 and 7. The two solid lines show fits to the predicted admittance curves are for model times of 12.6 and 13.6 m.y. when delamination is occurring. Dash-dot lines show bottom-loading curves, similar to those in Fig. 4.

Fig 1a

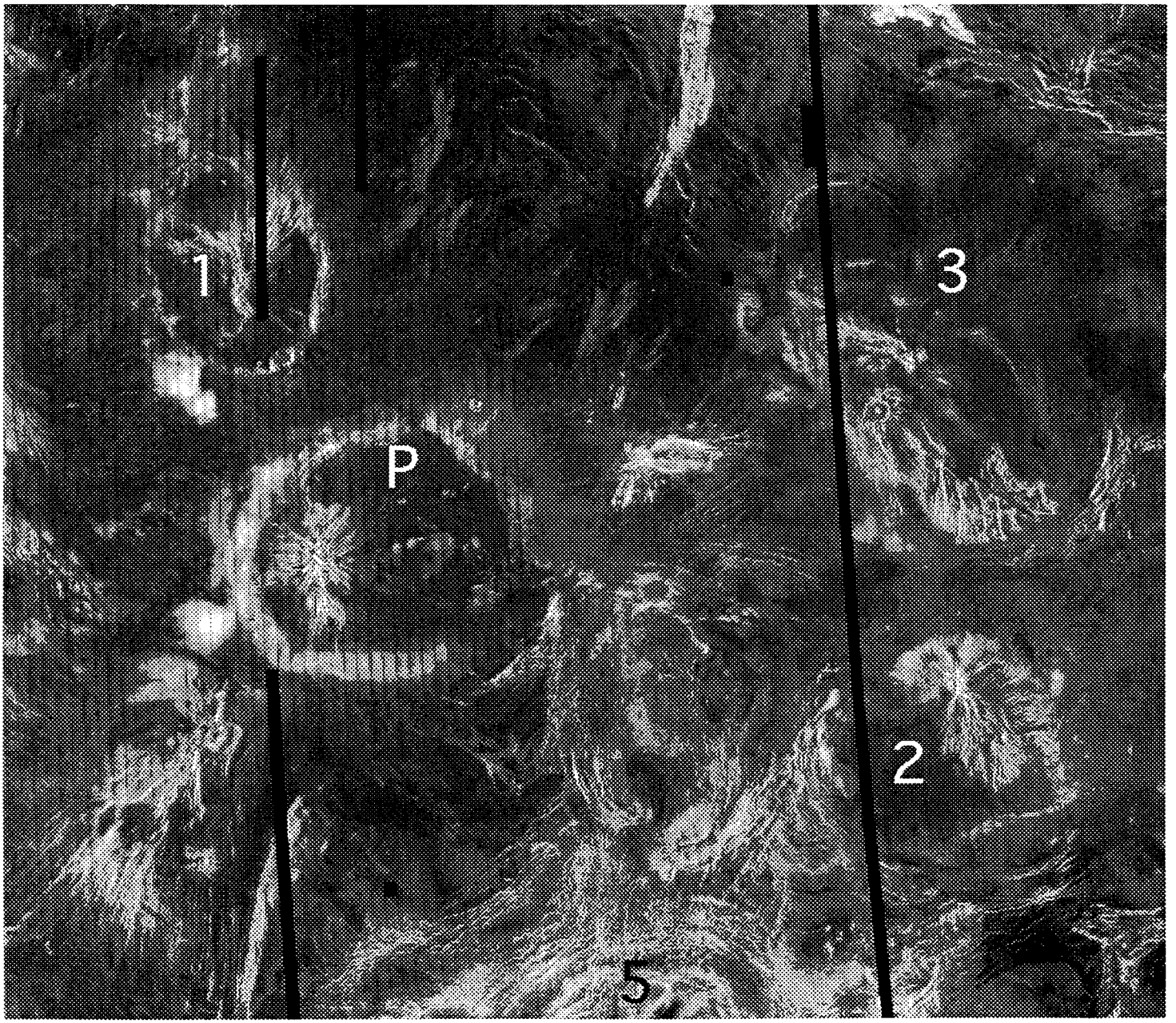
1
P
3
2
5


N
S
A
Su

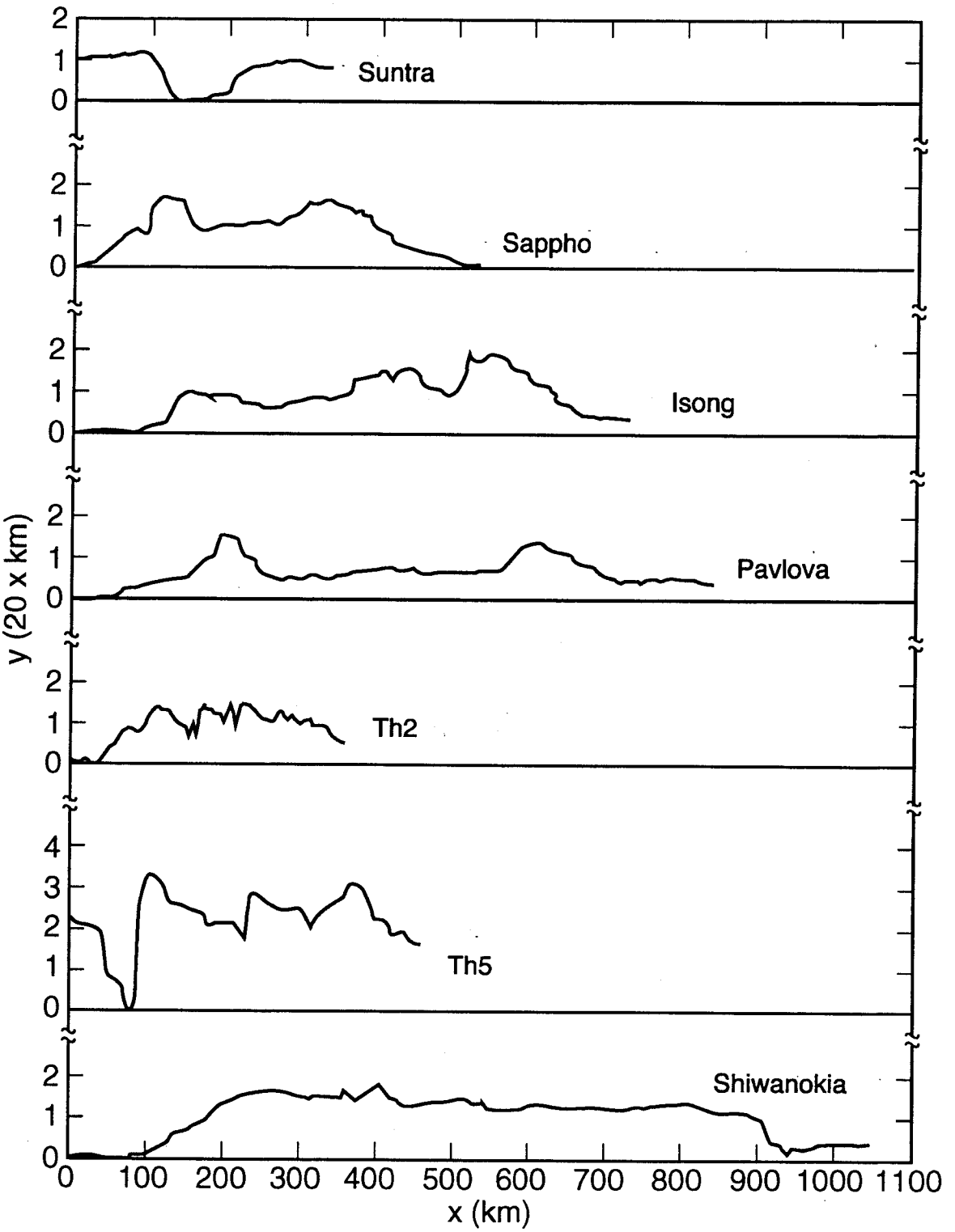
Suntra
Sappho
Isong
Pavlova
Th2
Th5
Shiwanokia
y (20 x km)
x (km)
0
100
200
300
400
500
600
700
800
900
1000
1100

Fig 2

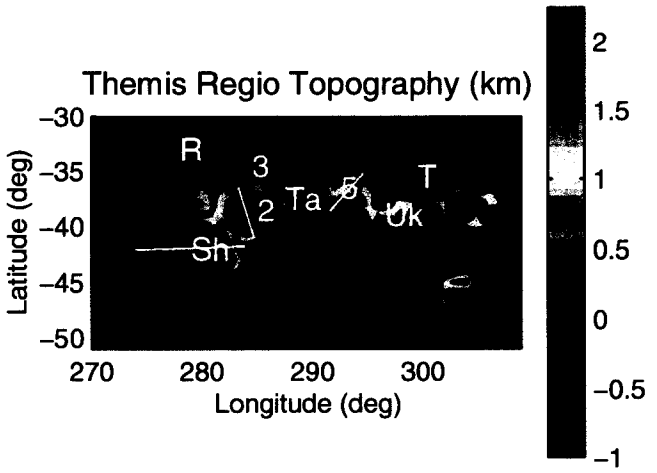
Themis Regio Topography (km)
R
3
2
Ta
T
Uk
Sh
Latitude (deg)
−30
−35
−40
−45
−50
270
280
290
300
Longitude (deg)
2
1.5
1
0.5
0
−0.5
−1

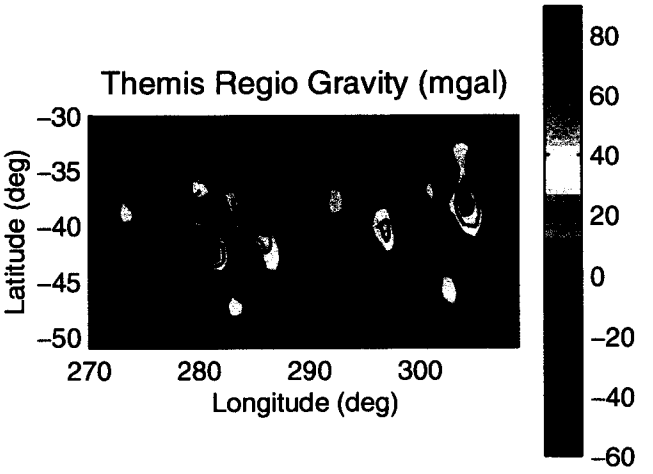
Themis Regio Gravity (mgal)
Latitude (deg)
−30
−35
−40
−45
−50
270
280
290
300
Longitude (deg)
80
60
40
20
0
−20
−40
−60

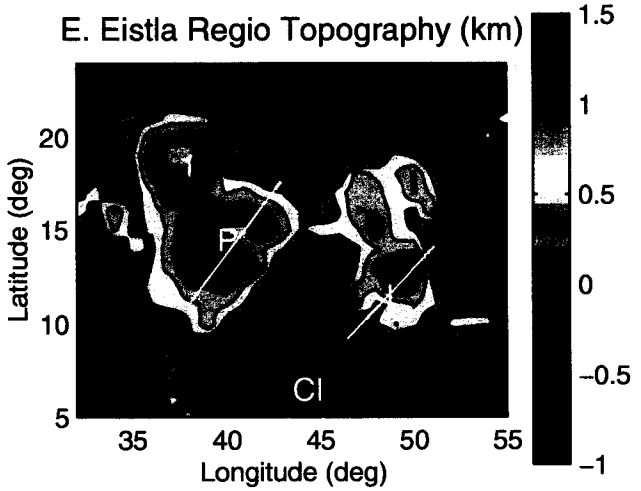
E. Eistla Regio Topography (km)
Pf
Cl
Latitude (deg)
20
15
10
5
35
40
45
50
55
Longitude (deg)
1.5
1
0.5
0
−0.5
−1

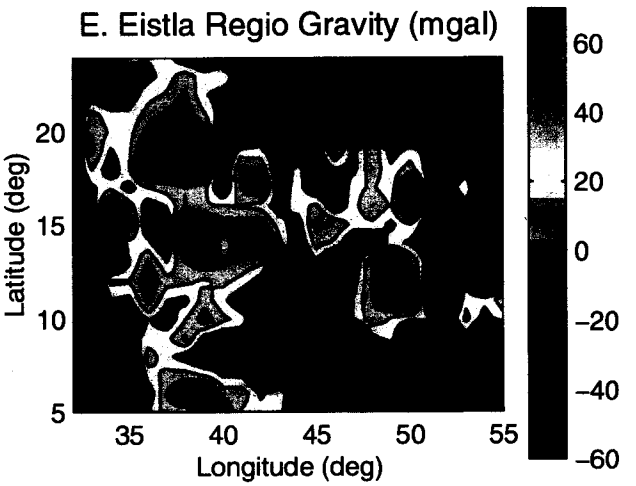
E. Eistla Regio Gravity (mgal)
Latitude (deg)
20
15
10
5
35
40
45
50
55
Longitude (deg)
60
40
20
0
−20
−40
−60

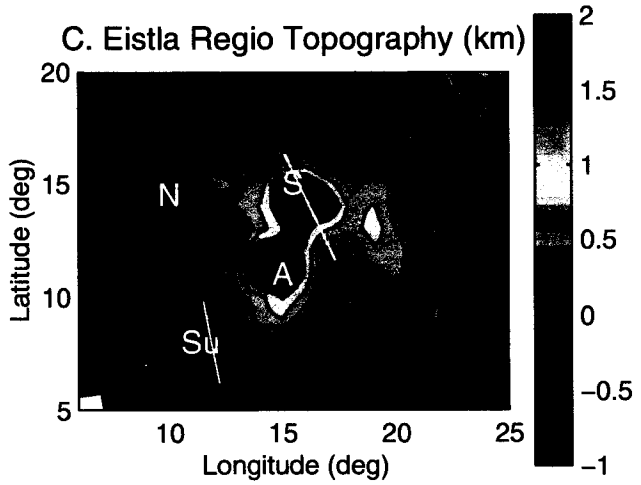
C. Eistla Regio Topography (km)
N
S
A
Su
Latitude (deg)
20
15
10
5
10
15
20
25
Longitude (deg)
2
1.5
1
0.5
0
−0.5
−1

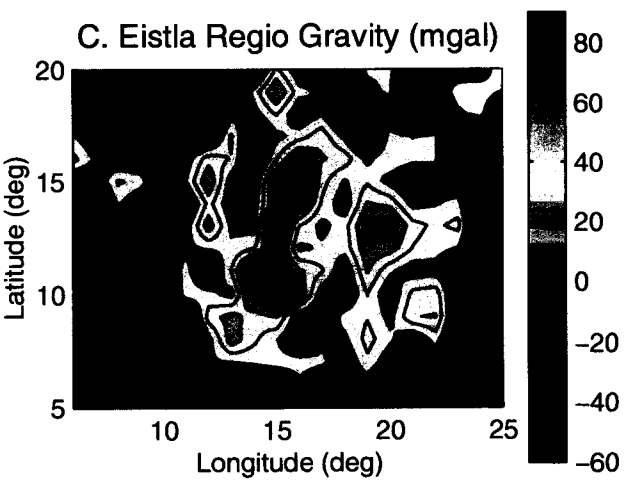
C. Eistla Regio Gravity (mgal)
Latitude (deg)
20
15
10
5
10
15
20
25
Longitude (deg)
80
60
40
20
0
−20
−40
−60

Fig 2

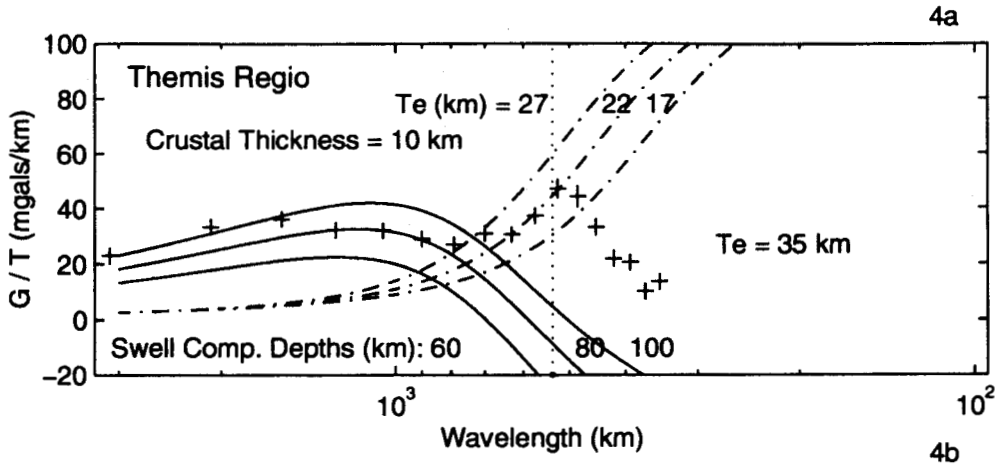
4a
Themis Regio
Te (km) = 27
22
17
Crustal Thickness = 10 km
Te = 35 km
Swell Comp. Depths (km): 60
80
100
G / T (mgals/km)
Wavelength (km)

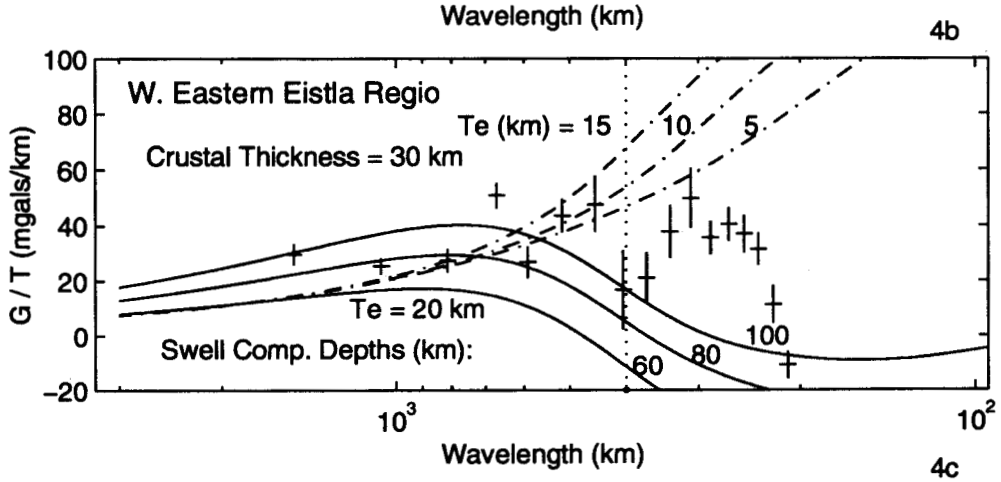
4b
W. Eastern Eistla Regio
Te (km) = 15
10
5
Crustal Thickness = 30 km
Te = 20 km
Swell Comp. Depths (km):
60
80
100
G / T (mgals/km)
Wavelength (km)

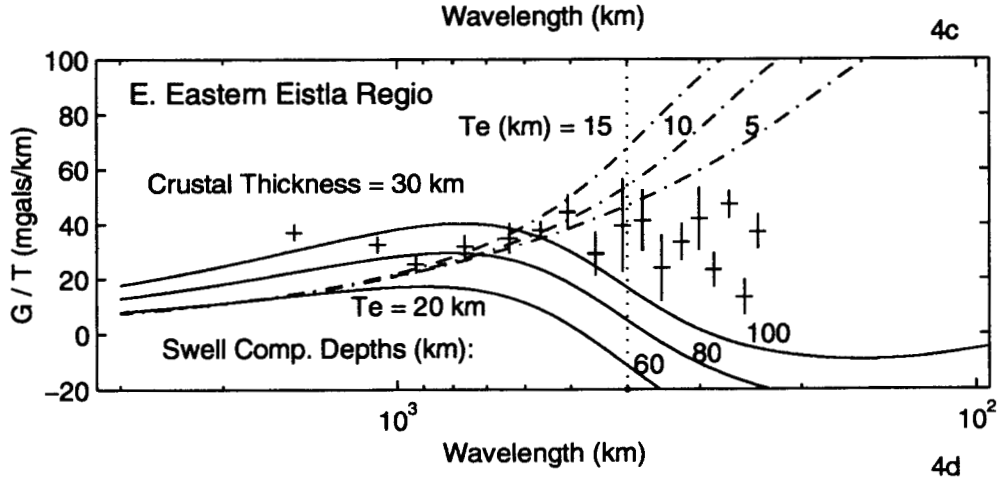
4c
E. Eastern Eistla Regio
Te (km) = 15
10
5
Crustal Thickness = 30 km
Te = 20 km
Swell Comp. Depths (km):
60
80
100
G / T (mgals/km)
Wavelength (km)

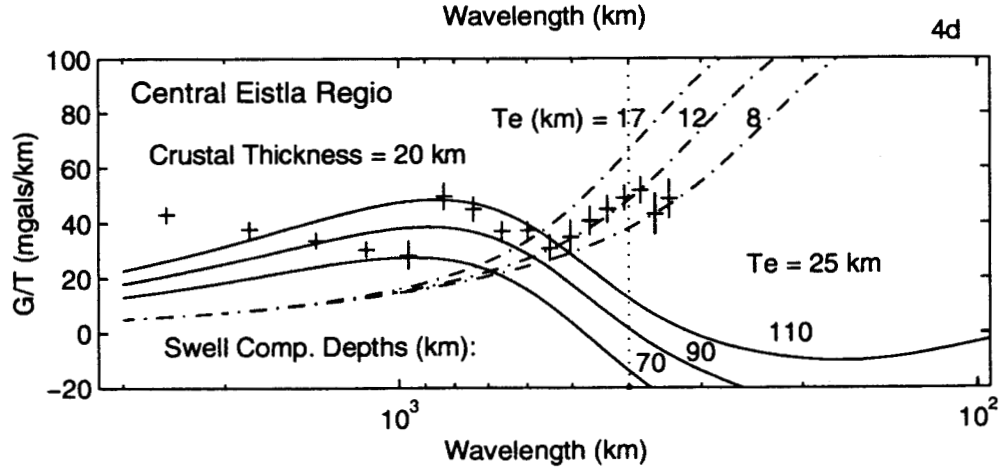
4d
Central Eistla Regio
Te (km) = 17
12
8
Crustal Thickness = 20 km
Te = 25 km
Swell Comp. Depths (km):
70
90
110
G/T (mgals/km)
Wavelength (km)

Fig 4

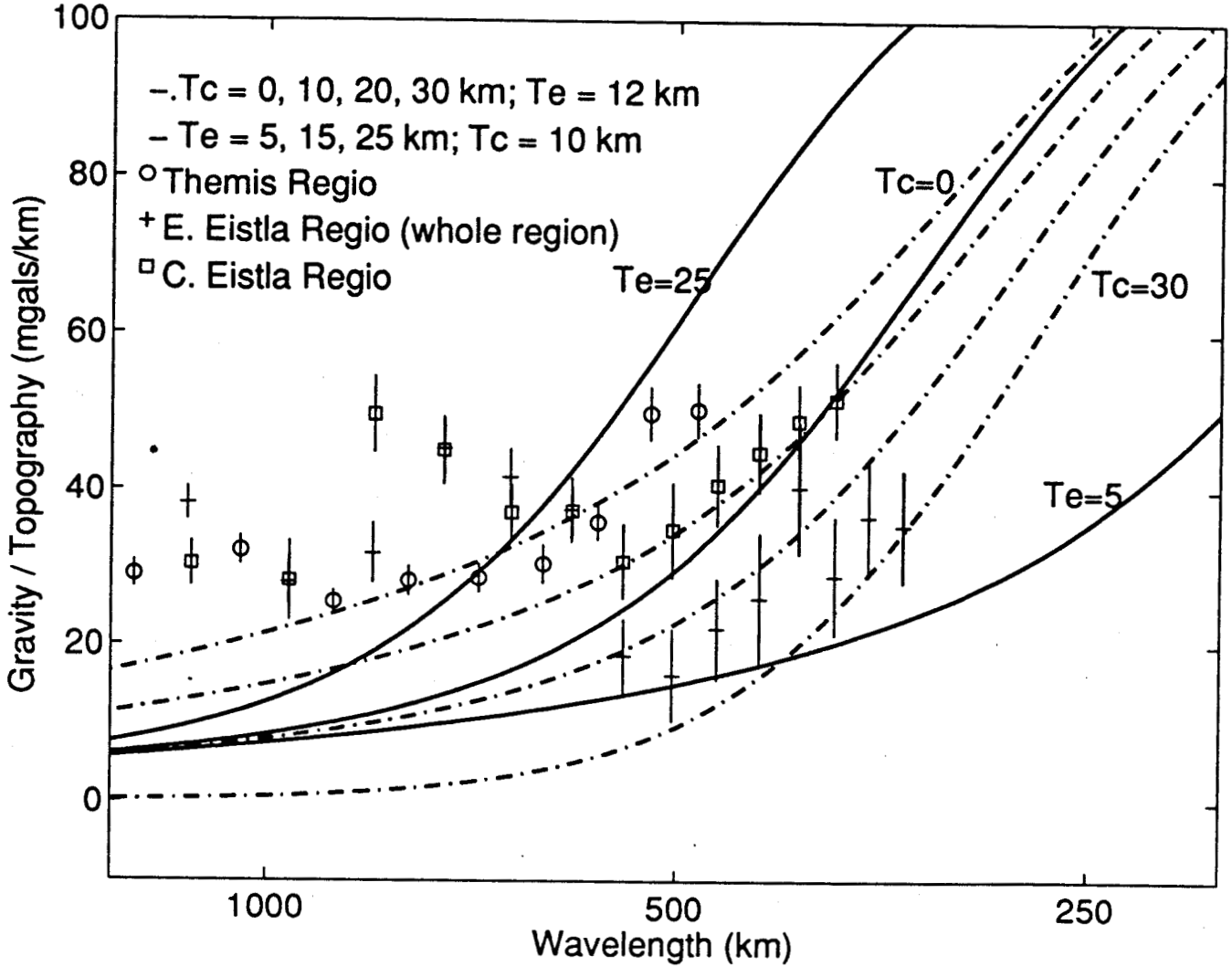
100
80
60
40
20
0
Gravity / Topography (mgals/km)
1000
500
250
Wavelength (km)
–.Tc = 0, 10, 20, 30 km; Te = 12 km
– Te = 5, 15, 25 km; Tc = 10 km
Themis Regio
E. Eistla Regio (whole region)
C. Eistla Regio
Tc=0
Tc=30
Te=25
Te=5

Figure 5

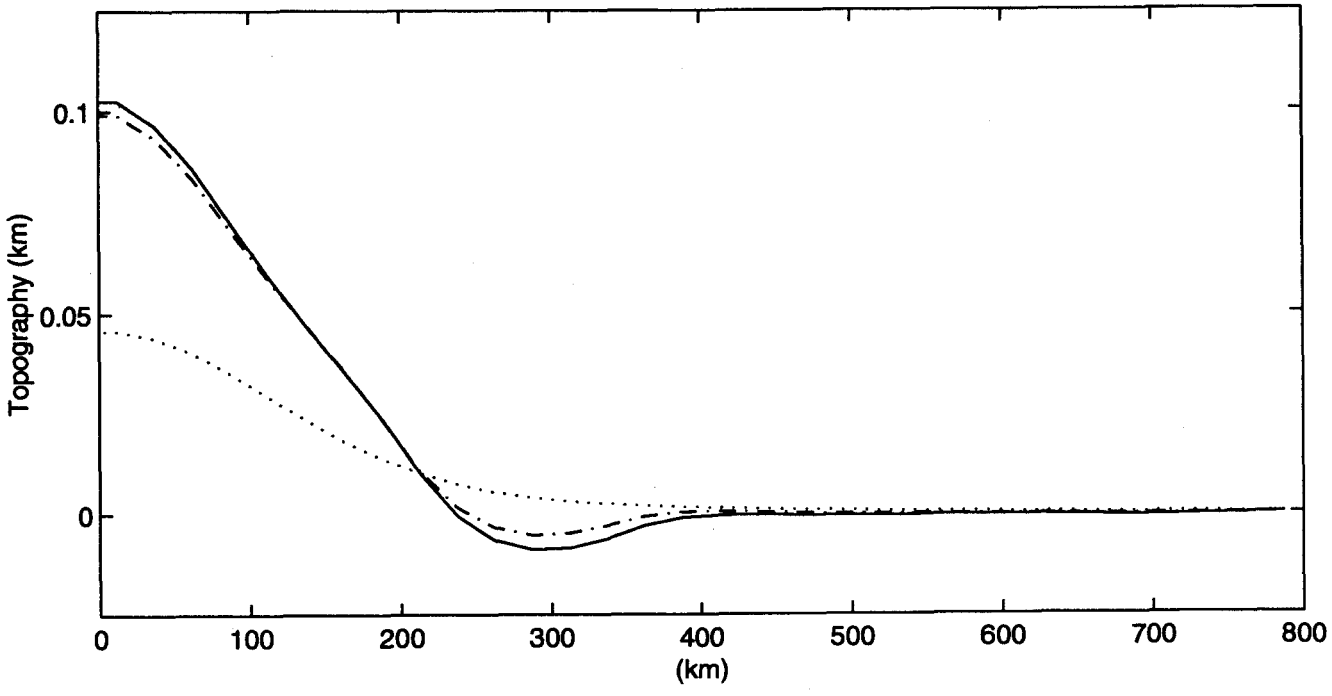

Fig 7

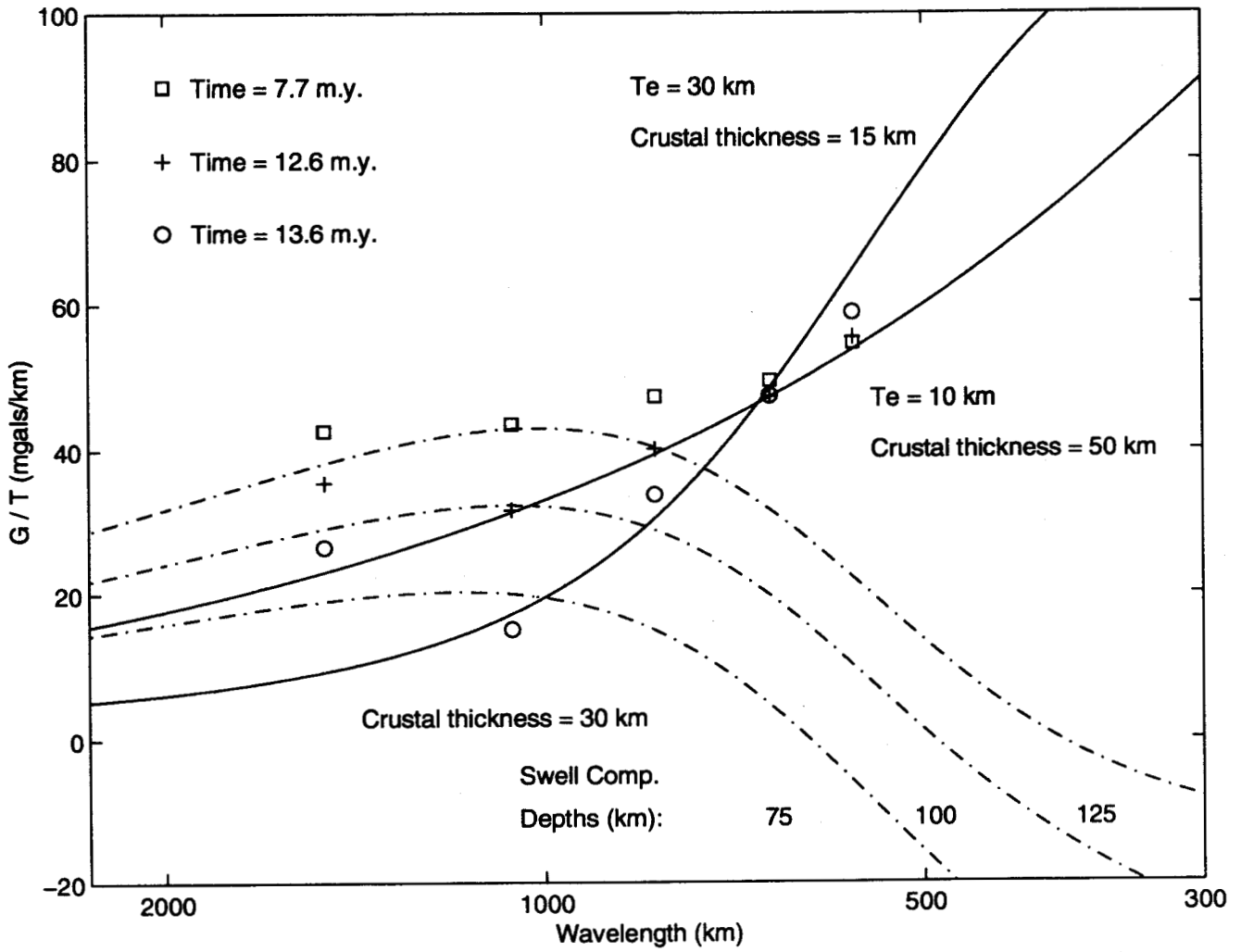
Time = 7.7 m.y.
Time = 12.6 m.y.
Time = 13.6 m.y.
Te = 30 km
Crustal thickness = 15 km
Te = 10 km
Crustal thickness = 50 km
Crustal thickness = 30 km
Swell Comp.
Depths (km):
75
100
125
G / T (mgals/km)
Wavelength (km)
100
80
60
40
20
0
-20
2000
1000
500
300

Fig 8